The Ca²⁺-activated Cl⁻ channel TMEM16B shapes the response time course of olfactory sensory neurons

Johannes Reisert[1] (iD), Simone Pifferi[2] (iD), Giorgia Guarneri[3], Chiara Ricci[3] (iD), Anna Menini[3] and Michele Dibattista[4] (iD)

[1] *Monell Chemical Senses Center, Philadelphia, PA, United States*
[2] *Department of Experimental and Clinical Medicine, Università Politecnica delle Marche, Ancona, Italy*
[3] *Neurobiology Group, SISSA, Scuola Internazionale Superiore di Studi Avanzati, Trieste, Italy*
[4] *Department of Translational Biomedicine and Neuroscience, University of Bari Aldo Moro, Bari, Italy*

Handling Editors: Nathan Schoppa & Conny Kopp-Scheinpflug

The peer review history is available in the Supporting Information section of this article (https://doi.org/10.1113/JP286959#support-information-section).
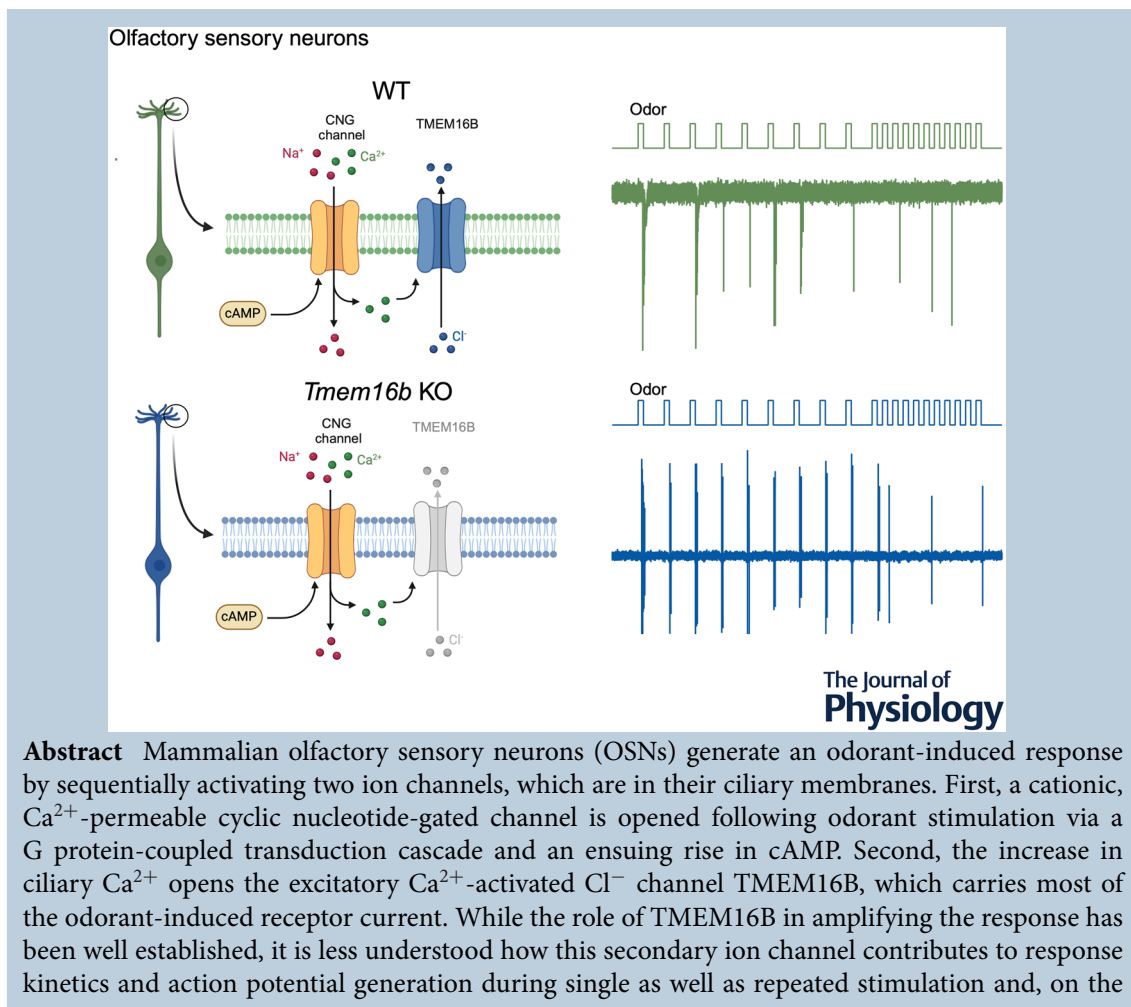
Abstract Mammalian olfactory sensory neurons (OSNs) generate an odorant-induced response by sequentially activating two ion channels, which are in their ciliary membranes. First, a cationic, Ca²⁺-permeable cyclic nucleotide-gated channel is opened following odorant stimulation via a G protein-coupled transduction cascade and an ensuing rise in cAMP. Second, the increase in ciliary Ca²⁺ opens the excitatory Ca²⁺-activated Cl⁻ channel TMEM16B, which carries most of the odorant-induced receptor current. While the role of TMEM16B in amplifying the response has been well established, it is less understood how this secondary ion channel contributes to response kinetics and action potential generation during single as well as repeated stimulation and, on the

---

other hand, which response properties the cyclic nucleotide-gated (CNG) channel determines. We first demonstrate that basic membrane properties such as input resistance, resting potential and voltage-gated currents remained unchanged in OSNs that lack TMEM16B. The CNG channel predominantly determines the response delay and adaptation during odorant exposure, while the absence of the Cl^- channels shortens both the time the response requires to reach its maximum and the time to terminate after odorant stimulation. This faster response termination in *Tmem16b* knockout OSNs allows them, somewhat counterintuitively despite the large reduction in receptor current, to fire action potentials more reliably when stimulated repeatedly in rapid succession, a phenomenon that occurs both in isolated OSNs and in OSNs within epithelial slices. Thus, while the two olfactory ion channels act in concert to generate the overall response, each one controls specific aspects of the odorant-induced response.

Corresponding authors A. Menini: Neurobiology Group, SISSA, Scuola Internazionale Superiore di Studi Avanzati, Trieste, Italy.   Email: menini@sissa.it

M. Dibattista: Department of Translational Biomedicine and Neuroscience, University of Bari Aldo Moro, Bari, Italy. Email: michele.dibattista@uniba.it

Abstract figure legend Odorant signal transduction transforms a chemical signal into an electrical one within the cilia of olfactory sensory neurons (OSNs). This process begins with the activation of an odorant receptor and culminates in the activation of cyclic nucleotide-gated (CNG) channels, facilitating Na^+ and Ca^{2+} influx. Subsequently, Ca^{2+} activates chloride channels (TMEM16B), further depolarizing the cell. While CNG and TMEM16B channels together generate the overall response, they control distinct aspects of it. CNG channels manage response delay and adaptation to odorant exposure, while TMEM16B amplifies the response and influences the time needed to reach peak and termination. OSNs lacking TMEM16B exhibit quicker response termination, enhancing their ability to fire action potentials during rapid, repeated odorant stimuli. Thus, CNG and TMEM16B channels have unique yet complementary roles in determining the kinetics and reliability of odorant-induced responses in OSNs. Created with BioRender.com

Key points

- Mammalian olfactory sensory neurons (OSNs) generate odorant-induced responses by activating two ion channels sequentially in their ciliary membranes: a Na^+, Ca^{2+}-permeable cyclic nucleotide-gated (CNG) channel and the Ca^{2+}-activated Cl^- channel TMEM16B.
- The CNG channel controls response delay and adaptation during odorant exposure, while TMEM16B amplifies the response and influences the time required for the response to reach its peak and terminate.
- OSNs lacking TMEM16B display faster response termination, allowing them to fire action potentials more reliably during rapid repeated stimulation.
- The CNG and TMEM16B channels have distinct and complementary roles in shaping the kinetics and reliability of odorant-induced responses in OSNs.

Johannes Reisert and **Simone Pifferi's** research is driven by trying to understand how odours influence our behaviour. In particular, their interest lies in one of the first steps in this process, which is understanding how olfactory sensory neurons encode the presence of odorants into, ultimately, action potentials to be conveyed to the brain. Their first in-person meeting was Simone's PhD exam (successful!) which Johannes had the pleasure to attend as an examiner. Since then, their common interest and complementary expertise in channel biophysics and cell physiology, respectively, has led to an enjoyable, lasting and productive collaboration across continents addressing how ion channels in olfactory sensory neurons contribute to our odour perception.

Introduction

Ethologically relevant odour-guided tasks, such as finding food, are crucial for an animal's survival; failing to do so would cause death. Locating food based on its odour cues is dependent on a series of mechanisms starting at the very periphery of the olfactory system: odorant transduction mechanisms in olfactory sensory neurons (OSNs), which are located in the olfactory epithelium in the nasal cavity (Genovese et al., 2021; Kleene, 2008; Pifferi et al., 2012; Tirindelli et al., 2009). Inhaled odorants are detected by OSNs and are transduced first into a receptor current that then triggers action potentials that are conveyed to the olfactory bulb and secondary neurons (Cang & Isaacson, 2003; Gire et al., 2012; Spors et al., 2006; Tan et al., 2015). Olfactory transduction occurs in OSN cilia (Fig. 1), which reach from the OSN dendrite into the mucus that lines the nasal cavity. Cilia contain the molecular machinery required for odour detection, which begins with the activation of an odorant receptor following odorant binding (Buck & Axel, 1991; Malnic et al., 1999). Adenylyl cyclase III (ACIII) (Bakalyar & Reed, 1990), via the G protein G_{olf} (Jones & Reed, 1989), increases cAMP which opens the olfactory cyclic nucleotide-gated (CNG) channel (Nakamura & Gold, 1987). This channel conducts Ca^{2+} and thus raises ciliary Ca^{2+} levels. Interestingly, Ca^{2+} then activates a Ca^{2+}-activated Cl^- channel TMEM16B (also known as Anoctamin 2) (Billig et al., 2011; Hengl et al., 2010; Kleene & Gesteland, 1991; Kurahashi & Yau, 1993; Li et al., 2018; Lowe & Gold, 1993; Rasche et al., 2010; Sagheddu et al., 2010; Stephan et al., 2009). As ciliary Cl^- is high and mucosal Cl^- is of around equal concentration (Kaneko et al., 2004), this channel is excitatory and carries about 80–90% of the transduction current, thus largely amplifying the initial CNG current (Boccaccio & Menini, 2007; Kleene, 1993; Reisert et al., 2005). Action potentials driven by the depolarizing transduction currents are typically only generated at the onset of the odorant-induced response with the amplitude of the action potentials quickly decreasing within an action potential train (Reisert & Matthews, 2001). This is most likely due to inactivation of voltage-gated Na^+ and Ca^{2+} channels during the strong depolarization in OSNs, which have a very high input resistance (Kawai et al., 1997; Trotier, 1994). Mouse OSNs often only generate two or three action potentials when exposed to odorants (Reisert & Matthews, 2001).

The contribution of the amplitude and kinetics of odorant transduction to olfactory-driven behaviour is not very well understood. Mouse models lacking G_{olf}, ACIII and the main subunit of the CNG channel, CNGA2, showed hardly any odorant responses, and pups had poor survival rates because of their inability to locate food and therefore feed (Belluscio et al., 1998; Brunet et al., 1996; Wong et al., 2000). The lack of odorant-induced response precluded more detailed analysis of their role in response kinetics. The last component in the series of events that lead to the generation of the transduction currents is the Ca^{2+}-activated Cl^- channel TMEM16B and although its role in amplifying the receptor current is well established, its contribution to olfactory-driven behaviour has been less clear cut. Originally it was concluded that TMEM16B might serve little to no role in olfactory behaviour (Billig et al., 2011), with a later more nuanced evaluation of its role suggesting that it alters OSN action potential generation, axonal targeting
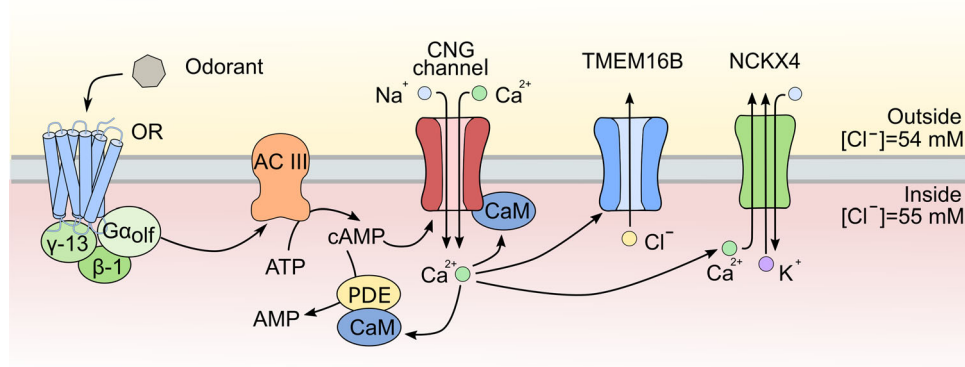

Figure 1. Olfactory signal transduction
When an odorant binds to an olfactory receptor (OR), it activates a trimeric G protein, which subsequently stimulates adenylyl cyclase III (ACIII) to produce cAMP. This cAMP opens cyclic nucleotide-gated (CNG) channels, allowing the influx of Na^+ and Ca^{2+} ions. The increase in intracellular Ca^{2+} then activates the TMEM16B chloride (Cl^-) channel. Olfactory sensory neurons (OSNs) maintain a high intraciliary chloride concentration ([Cl^-]) of 55 mM, while the [Cl^-] in the mucus is around 54 mM (Kaneko et al., 2004). Thus, the driving force for Cl^- at the resting membrane potential of OSNs favours its efflux. Additionally, Ca^{2+} binds to calmodulin (CaM), which reduces the sensitivity of the CNG channels to cAMP and activates phosphodiesterase PDE1C. Finally, Ca^{2+} is removed from the cell via the Na^+/Ca^{2+} exchanger NKCX4. [Colour figure can be viewed at wileyonlinelibrary.com]

of OSN axons to the olfactory bulb and bulbar activity, and odour-guided search tasks, in particular for novel odours (Neureither et al., 2017; Pietra et al., 2016; Zak et al., 2018). Therefore, the role of the Cl^- channel in odour response magnitude and kinetics to shape OSN physiology, in particular in longer and repeated odour stimulation and ultimately behaviour, is important to consider (Guarneri et al., 2023). In general, the kinetics of the peripheral odorant responses must be finely tuned to repeated odorant stimulations at breathing rates at rest or during high-frequency sniff bouts (Ghatpande & Reisert, 2011). Therefore, understanding each aspect of the odorant response (i.e. termination, adaptation, action potential frequency and potential number as well as train duration) would help us to define the contribution of peripheral odour coding to overall olfactory coding. To tackle those points, we used a mouse model lacking TMEM16B to better understand response kinetics and odorant-induced adaptation. In addition, we designed OSN stimulation paradigms to mimic sniffing pattern to study how isolated OSNs generate action potentials as well as OSNs in slices of the olfactory epithelium.

Methods

Ethical approval

Mice were handled in accordance with the guidelines of the Italian Animal Welfare Act and European Union guidelines on animal research, under a protocol approved by the ethics committee of SISSA or in accordance with methods approved by the Animal Care and Use Committees of the Monell Chemical Senses Center (conforming to National Institutes of Health guidelines). Mice had access to standard mouse chow and water *ad libitum* and were on a 12 h light/dark cycle. Every effort was made to reduce the number of animals used. C57BL/6 mice of both sexes (age range, 2−3 months) were anaesthetized with CO_2 and decapitated. Mice were transferred to a cage (height/width/length, 8 × 10 × 12 cm), and 100% CO_2 was slowly injected into the cage until the animal stopped breathing and no longer displayed pedal reflex (near 3 min; gas flow rate, ∼20% of chamber volume/min).

The investigators understand the ethical principles under which *The Journal of Physiology* operates, and the work within this study fully complies with *The Journal*'s animal ethics checklist.

Suction pipette experiments

For suction pipette experiments, heterozygous *Tmem16b* breeder mice were obtained from T. Jentsch, Max-Delbrück-Centrum für Molekulare Medizin, Berlin,

Germany (Billig et al., 2011) and bred to obtain WT and *Tmem16b* KO mice. Adult mice of either sex were killed by CO_2 inhalation and decapitated. The head was split sagittally along the midline and the olfactory epithelium was removed. The tissue was stored in glucose-containing Ringer solution at 4°C until further use. The Ringer solution contained in mM: 140 NaCl, 5 KCl, 1 $MgCl_2$, 2 $CaCl_2$, 0.01 EDTA, 10 HEPES and 10 glucose. The pH was adjusted to 7.5 with NaOH. Odorants, cineole and acetophenone (Sigma), were dissolved in Ringer solution at the stated concentrations.

Odorant-induced responses from isolated OSNs were recorded using the suction pipette technique as previously described (Dibattista & Reisert, 2018; Lowe & Gold, 1991; Ponissery Saidu et al., 2012). OSNs were isolated by placing olfactory epithelium in an Eppendorf tube filled with Ringer solution, followed by gentle vortexing. OSNs were allowed to settle in the recording chamber and subsequently sucked into the tip of the recording pipette. Currents were recorded with a Warner PC-501A patch-clamp amplifier, digitized using a Power1401 II A/D converter and Signal acquisition software (Cambridge Electronic Design). Currents were acquired twice, once filtered at 0−50 Hz to display the receptor current and once at 0–5 kHz to resolve the fast biphasic action currents that drive the action potentials. The sampling frequency was 10 kHz.

OSNs were exposed to odorants using the Perfusion Fast-Step solution changer (Warner Instrument Corporation). The tip of the recording pipette with the sucked OSN was transferred quickly across the interface of two neighbouring solution streams, which were heated to a mammalian body temperature of 37°C (Matthews, 1999).

Preparation of acute slices of mouse olfactory epithelium

Acute coronal slices of olfactory epithelia of P0−P4 mice were obtained with a method similar to that previously described by Henriques et al. (2019) and Agostinelli et al. (2021). Mice at this age are suitable for use since TMEM16B is already express at P0–P4 (Maurya & Menini, 2014; Maurya et al., 2015). For these experiments, we used *Tmem16b* KO mice kindly provided by Prof. Lily Jan (University of California, San Francisco, USA; Zhang et al., 2017). After the mouse was killed, the head without the skin was dissected and embedded in 3% low-grade agar prepared in Ringer solution once the solution had cooled to 38°C. After solidification the agar block was fixed in a glass Petri dish filled by oxygenated Ringer solution and a vibratome was used to cut coronal slices 300 μm thick (Vibratome 1000 Plus Sectioning System). The slices were kept in cold oxygenated Ringer solution until use.

Electrophysiological recordings from OSNs and stimuli presentation

Slices were viewed with an upright microscope (BX51WI, Olympus) equipped with a 40× water immersion objective with an additional 2× auxiliary lens. The recording chamber was continuously perfused with oxygenated Ringer solution at room temperature. Extracellular solutions were exchanged through an eight-in-one multibarrel perfusion pencil connected to a ValveLink 8.2 pinch-valve perfusion system (Automate Scientific). The bath was connected to an Ag/AgCl reference electrode through a 3 M KCl agar bridge. OSNs were identified by their morphology. The experiments were performed at room temperature (20–25°C). Patch pipettes were pulled from borosilicate capillaries (WPI) with a Narishige PC-10 puller.

In the whole-cell voltage-clamp configuration experiments the pipette had a resistance of 4–7 MΩ when filled with the intracellular solution. We used an intracellular solution composed of (in mM) 80 KGluconate, 60 KCl, 2 MgATP, 1 EGTA and 10 HEPES (adjusted to pH 7.2 with KOH) to measure the voltage-gated currents and the passive properties of the OSNs. The voltage-gated current was measured in voltage-clamp mode, holding the potential at −90 mV and applying a voltage step protocol from −100 mV to +40 mV in 10 mV increments. In voltage-clamp mode, we also evaluated the membrane input resistance. We held the potential of the cell at −90 mV and gave a negative pulse of 20 mV. In these conditions, the voltage-gated currents are not activated (Dibattista et al., 2008). In current-clamp mode (without injecting current), we measured the resting membrane potential. To isolate the Cl⁻ current contribution, we used an intracellular solution composed of (in mM) 13 KCl, 132 KGluconate, 4 MgCl$_2$, 0.5 EGTA and 10 HEPES (adjusted to pH 7.2 with KOH). In this way, the reversal potential for Cl⁻, after online correction for the liquid junction potential, corresponds to the holding potential of −50 mV. In this condition the current is mainly mediated by CNG channels.

Extracellular recordings from the soma of OSNs were obtained in the loose-patch configuration using a pipette with a resistance of 3–4 MΩ when filled with Ringer solution. During the experiments the seal resistances were 30–50 MΩ. Loose-patch experiments were made in voltage-clamp mode with a holding potential of 0 mV. The recordings were performed using a MultiClamp 700B amplifier controlled by Clampex 10.6 via Digidata 1550B (Axon Instrument, USA). Data were low-pass filtered at 2 kHz and sampled at 10 kHz.

The cells were stimulated with a mix of odorants composed of heptanal, isoamyl acetate, acetophenone, cineole and eugenol. Each odorant was prepared as a 5 M stock in dimethyl sulfoxide (DMSO) and on the day of experiments was diluted in Ringer solution to reach the final concentration of 100 µM each. We used 3-isobutyl-1-methylxanthine (IBMX). IBMX is a phosphodiesterase (PDE) inhibitor which induces an increase of the cAMP concentration in a subpopulation of OSNs. It was prepared weekly and used at the concentration of 1 mM dissolved directly in Ringer solution without the use of DMSO. At this concentration, IBMX elicits responses with kinetics similar to those induced by odorants (Reisert et al., 2007).

Data analysis

IgorPro software (Wavemetrics) was used for the data analysis and to make the figures. Data are given as means ± SD. Normal distribution of the data was tested with the Shapiro–Wilk test. The homogeneity of the variance was tested using Levene's test. If the data are normally distributed and with the same variance, statistical significance was determined using unpaired homoscedastic Student's *t* test or two-way ANOVA. If data presented with a different variance, an unpaired different variance Student's *t* test was used. For not normally distributed data, the Mann–Whitney *U* test was used. *P* values of $P < 0.05$ were considered statistically significant. The loose-patch recordings were filtered offline with a high-pass filter at 5 Hz to correct for baseline drifts. Spikes were detected using an event detection algorithm setting an arbitrary threshold and then were confirmed by shape examination.

Results

The absence of Cl⁻ channels does not alter the basic biophysical properties of OSNs

We sought to understand whether the removal of the Cl⁻ channel would affect the biophysical properties of OSNs. First, using the whole-cell patch-clamp configuration, we recorded both inward and outward voltage-gated currents from OSNs in olfactory epithelia slices and found that they were similar in their amplitude and their voltage dependency between the *Tmem16b* KO and the WT (Fig. 2*A,B*). Then, we measured the input resistance and resting membrane potential of OSNs from WT and *Tmem16b* KO mice and found that those were not different (Fig. 2*C,D*).

Although we found no differences in the biophysical properties we measured, we previously showed that in *Tmem16b* KO OSNs the transduction current is dramatically reduced (Pietra et al., 2016). Here, we confirmed this previous result by stimulating for 1 s with the phosphodiesterase inhibitor IBMX (1 mM). We set the holding potential to −50 mV, the equilibrium potential for

Cl⁻ with our solutions (see *Methods*) and the transduction currents in WT and KO OSNs were similar in amplitude (Fig. 2*E,F*) between WT and *Tmem16b* KO. Switching the holding potential to −90 mV greatly amplified the transduction current revealing the contribution of the Cl⁻ currents (Fig. 2*E* tangerine trace) in the WT. In the

KO, there were no differences between the transduction currents recorded at different holding potentials (Fig. 2*F*) and the ratio between current amplitudes at −90 mV and −50 mV is close to 1 (Fig. 2*G*) in *Tmem16b* KO while it was increased threefold in the WT. Altogether, these results indicate that the absence of Cl⁻ current in
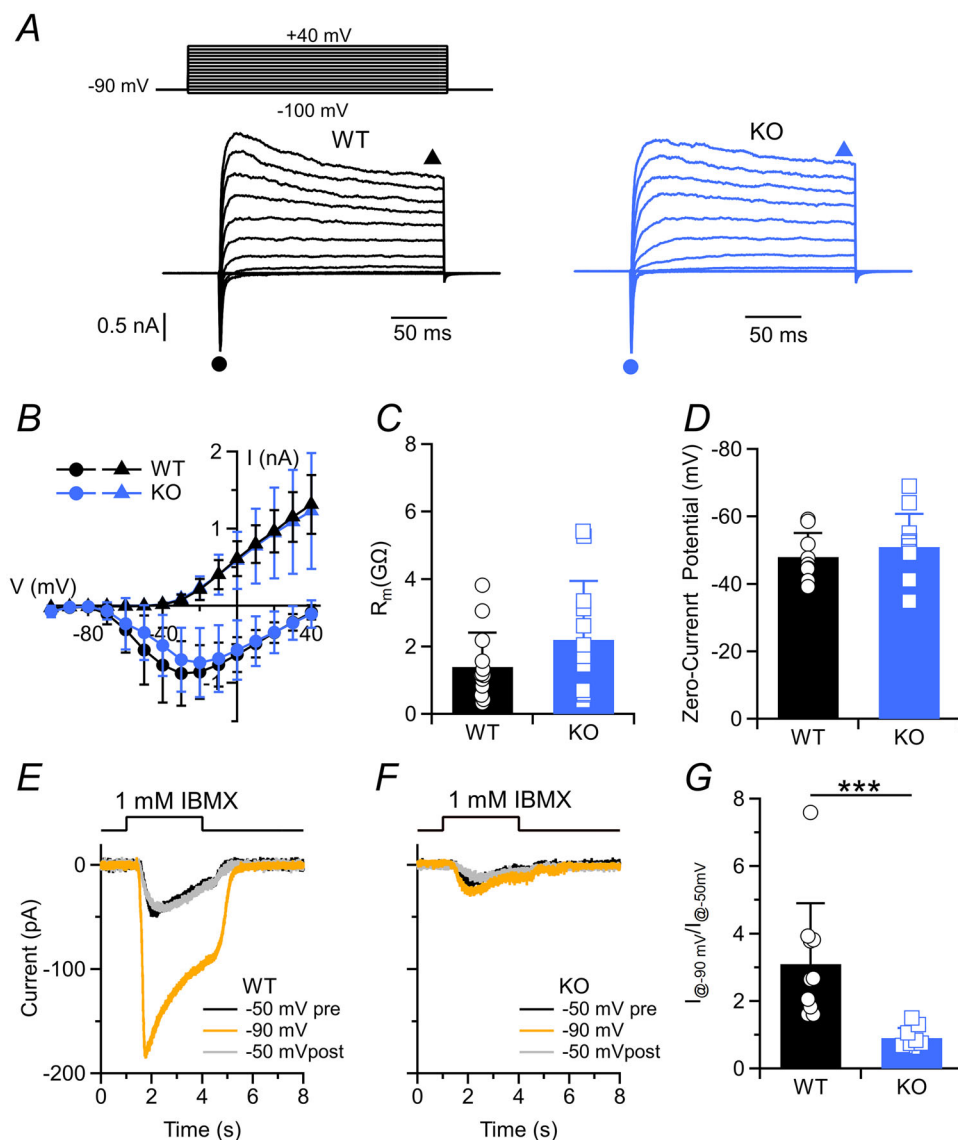

Figure 2. *Tmem16b* deletion abolishes the transduction Cl⁻ current without affecting the voltage-gated currents and membrane properties of olfactory sensory neurons (OSNs)

A, representative whole-cell voltage-clamp recordings of OSNs in olfactory epithelia slices from WT and *Tmem16b* KO mice. Voltage steps of 200 ms duration were given from a holding voltage of −90 mV to voltages between −100 and +40 mV in 10 mV steps. *B*, average ± SD of the *I–V* relationships of inward currents (circles) and steady-state outward current (triangles) from WT (black, $n = 14$) and *Tmem16b* KO (blue $n = 13$) OSNs. Values were taken at the negative peak and at the end of voltage step as indicated by the symbols in *A* ($P = 0.73$ unpaired *t* test for inward current; $P = 0.64$ *U* test for outward current). Scatter plot with averages ± SD of input membrane resistance (*C*) and zero-current membrane potential (*D*) of WT and *Tmem16b* KO OSNs (for R_m $n = 12–13$, $P = 0.24$, *U* test; for zero-current potential $n = 9–10$, $P = 0.28$, *U* test). Representative whole-cell recording of OSNs from WT (*E*) and *Tmem16b* KO mice (*F*) stimulated with IBMX (1 mM) at the indicated holding potential. *G*, scatter plot with averages ± SD of ratios of the IBMX-induced current at −9 mV and at −50 mV ($n = 10$ for WT and $n = 9$ for KO; $P = 2.16 \times 10^{-5}$ *U* test). [Colour figure can be viewed at wileyonlinelibrary.com]

OSNs does not change either their biophysical properties or the basic voltage-gated currents. On the other hand, the transduction current is greatly reduced in the OSNs from *Tmem16b* KO mice, confirming the significant contribution by the Cl⁻ current.

The Cl⁻ channel shapes kinetic parameters of the odorant response

To investigate how TMEM16B contributes to the odorant-induced response and its kinetics, we stimulated WT and *Tmem16b* KO OSNs with an odour mixture (100 μM of cineole and acetophenone each) and recorded the responses with the suction pipette technique. WT OSNs displayed the typical rapid rise of the suction current upon odorant exposure and decayed during the 1 s stimulation to decline gradually thereafter back to baseline (Fig. 3*A*). OSNs lacking TMEM16B responded with a similar delay, reached their peak current faster, but generated, as expected, a much smaller maximal current. The response current also declined during the 1 s stimulation and had a faster decline back to baseline at the end of stimulation than WT. To display and address action potential firing, we filtered odorant responses at a wider bandwidth (0–5 kHz). WT OSNs generated only a
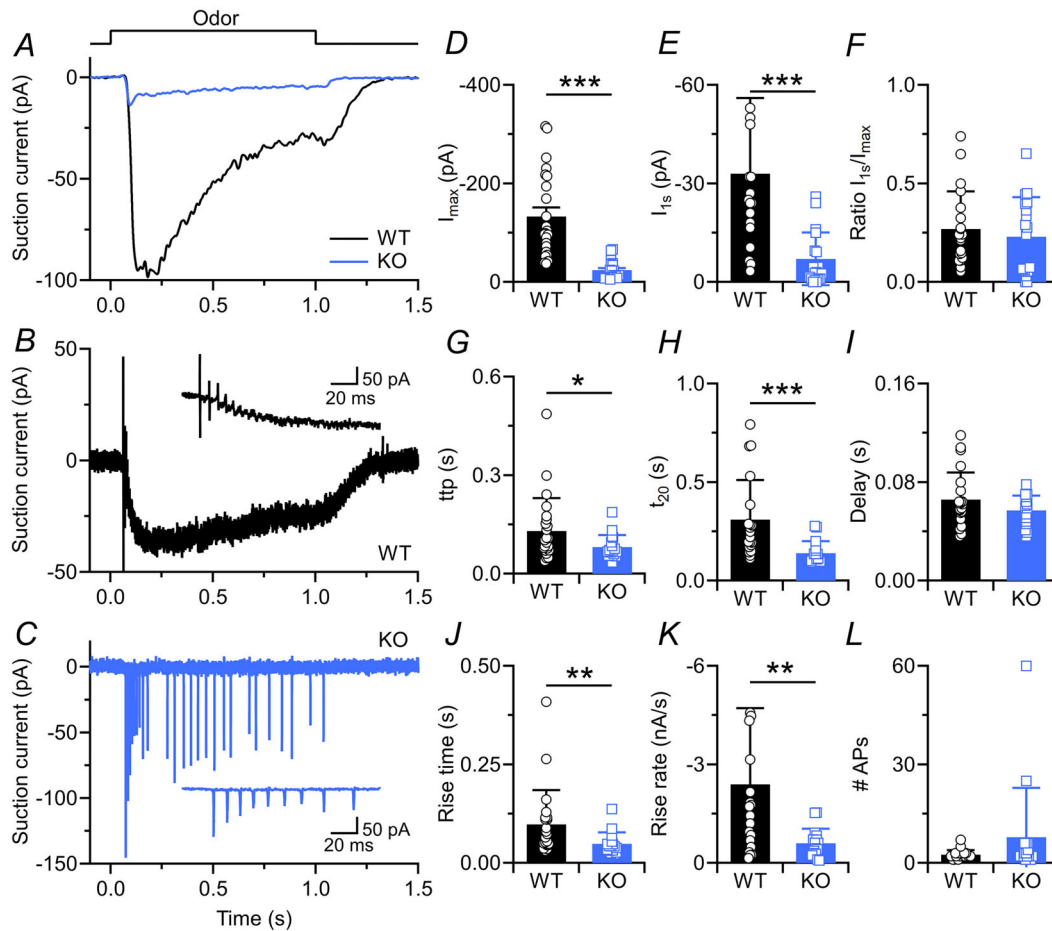

Figure 3. The lack of TMEM16B affects odorant response kinetics
A, olfactory sensory neurons (OSNs) were stimulated with 100 μM of cineole and acetophenone each for 1 s as indicated by the solution monitor on top. Current responses were recorded from isolated OSNs using the suction pipette technique and filtered at 0–50 Hz to display only the receptor current. *B* and *C*, WT and KO OSN responses filtered at the wide bandwidth of 0–5 kHz to also display action potentials. *D*, peak current I_{max} elicited by the odorant response. *E*, current I_{1s} at the end of the odorant stimulation. *F*, ratio of I_{1s} and I_{max}. *G*, time to peak (ttp), the time to reach I_{max} following odour onset. *H*, t_{20}, the time for the current to fall to 20% of I_{1s} from the end of stimulation. *I*, response delay measured as the time taken for the first action potential to be generated following odour onset. *J*, rise time, ttp minus delay. *K*, rise rate of the receptor current, I_{max} divided by rise time. *L*, number of action potentials generated during the 1 s stimulation. n = 20–23 OSNs for WT and 14–18 for KO (*D*: P = 8.9 × 10⁻⁶; *E*: P = 3.6 × 10⁻⁶; *F*: P = 0.47; *G*: P = 0.03; *H*: P = 7.6 × 10⁻⁴; *I*: 0.31; *J*: P = 0.003; *K*: P = 0.003; *L*: P = 0.3 * P < 0.05, ** P < 0.01, *** P < 0.001, U test). Bars indicate means and error bars are SD. [Colour figure can be viewed at wileyonlinelibrary.com]

few action potentials at the onset of stimulation (Fig. 3*B*) while KO OSNs could generate longer action potential trains (Fig. 3*C*).

On average, KO OSNs only generated a maximal current of around 20% of the WT OSNs (Fig. 3*D*). The current at 1 s, at the end of stimulation, was similarly reduced (Fig. 3*E*). This is reflected in a similar ratio of the current at 1 s when normalized to its maximal current (ratio I_{1s}/I_{max}, Fig. 3*F*). As the KO lacks the Cl^- current, this suggests that this decline in current response during the 1 s stimulation mostly depends on a reduction of the current through the CNG channels. Thus, the Cl^- channel itself might contribute little to this form of adaptation. Lack of Cl^- current curtailed the time the current required to reach its peak response (time to peak, ttp), from 130 ± 21 ms in WT to 81 ± 8 ms in the KO (Fig. 3*G*), indicating that while the current through the CNG channel might reach its maximum quickly, continuing, although decreasing, influx of Ca^{2+} can continue to increase ciliary Ca^{2+} and further increase the Cl^- current thereafter. At the termination of the response, the time required for the current to fall to 20% of the current at 1 s is also shortened from 310 ± 40 ms in the WT to 140 ± 20 ms in the KO (Fig. 3*H*), confirming the role of the Cl^- current in determining the response duration. Interestingly, the response delay, measured as the time between the onset of stimulation and the generation of the first action potential was unchanged in the KO compared with the WT and therefore seems to be mostly determined by the initial speed of activation of the CNG channel (Fig. 3*I*). The rise time (Fig. 3*J*), the duration from the response delay to the time to peak, as well as the rise rate (Fig. 3*K*), the peak current divided by the rise time, was larger in the WT than the KO. The number of action potentials generated in response to odour stimulation was not statistically different in WT and KO (Fig. 3*L*), although the KO in several cells showed an extreme prolongation of the action potential train.

The absence of Cl^- channels greatly reduce response amplitude without altering odorant sensitivity

We studied the role of TMEM16B in the odorant-induced dose response by exposing OSNs to an odorant mix of 3, 10, 30 and 100 μM of cineole and acetophenone each. In WT OSNs, the increase in the stimulus concentration led to increasingly larger receptor current responses (Fig. 4*A*), which also became longer. In KO OSNs, responses also increased, although at a much-reduced current level and the responses terminated quickly at the end of stimulation (Fig. 4*B*). Fig. 4*C* compares the average responses across WT and KO OSNs, with again the KO OSNs showing much smaller responses. We also asked if the sensitivity of KO OSNs might be reduced.

We normalized the dose–response relationship of each OSN to its response at 100 μM and averaged across all OSNs for WT and KO, respectively (Fig. 4*D*). The two dose–response relationships showed no shift relative to each other, suggesting that odorant sensitivity was largely unaltered in KO OSNs. The numbers of action potentials fired across the odorant concentrations used showed that KO OSNs generated more action potentials than the WT (two-way ANOVA, Fig. 4*E*).

Cl^- current contribution to the recovery from adaptation

As the odorant responses terminated more quickly in the KO OSNs, and the speed of response termination is a major determinant in the speed of recovery from odorant-induced adaptation (Dibattista & Reisert, 2016; Stephan et al., 2011), we performed double-pulse experiments where OSNs were exposed twice for 1 s with an increasing inter-pulse interval between the two stimulations. Fig. 5*A* shows such an experiment with an interval duration of 0.5 s for a WT OSN. In response to the first stimulation, the OSN generates a large response with action potentials also being generated at the onset of the response. At the end of the first stimulation, the current declined slowly and had not yet reached zero levels upon the beginning of the second stimulation. While the OSN still generated an increase, although small, in receptor current, it failed to generate action potentials at this point, most likely as voltage-gated Ca^{2+} and Na^+ channels were still inactivated from the preceding depolarization (Pietra et al., 2016; Trotier, 1994). In contrast (Fig. 5*B*), while the responses of the KO OSN were much smaller, the response to the first stimulation terminated quickly, allowing the OSN to reach its basal level of current and hence hyperpolarization to generate action potentials again when stimulated for the second time. To analyse the responses, we plotted the ratio of the second current response divided by the first against the inter-pulse interval (Fig. 5*C*). In both the WT and the KO, the response to the second stimulation progressively decreased with decreasing inter-pulse intervals, although the relative response size in the KO remained larger across all inter-pulse intervals, indicating that recovery from adaptation occurs on a faster timescale in the KO than the WT. To understand how action potential firing is affected, we calculated the chance of action potentials being generated when exposed to the second odour pulse. For long inter-pulse intervals, both WT and KO OSNs generated action potentials very reliably, but at inter-pulse intervals of 1 s and shorter, WT OSNs became less reliable in generating action potentials (Fig. 5*D*). For the KO, a drop in reliable action potential generation was only observed at the shortest inter-pulse interval of 0.25 s (Fig. 5*D*).

Odorant responses to different frequencies of stimulation

Given the previous result, we asked how WT and KO OSNs respond to a change in stimulation frequency from low (2 Hz, resembling breathing at rest) to a higher (5 Hz, resembling a more sniff-like) frequency. A WT OSN (Fig. 6A) reasonably tracked a 2 Hz stimulation pattern and generated action potentials in response to most stimulations but in this case failed to respond to the second and eighth stimulations. Its response reliability dropped even further when stimulated at 5 Hz thereafter. The KO OSN (Fig. 6B) generated action potentials to every stimulation at 2 Hz but did so with less reliability at 5 Hz. Fig. 6C compares the percentage of stimulations with fired action potentials at 2 Hz between WT and KO across odorant concentrations. The KO could maintain a high firing reliability of around and above 75% across the odorant concentrations, while in the case of the WT, with the exception of the lowest concentration, it stayed at around 50%, which was statistically lower than the KO.

At 5 Hz, both WT and KO showed low firing reliability of around 25%. Thus, while at lower stimulation frequencies KO OSNs are more reliable, this difference no longer observed at 5 Hz.

We sought to extend the previous sets of data by performing experiments using slices from olfactory epithelia and recorded using the loose-patch configuration. Similar to the suction pipette recordings, this configuration does not alter the intracellular milieu and additionally avoids any isolation-induced artefact. We applied five repetitive 1 s odour stimulations with an inter-pulse interval of 0.5 s, a similar recovery interval as used during the 2 Hz stimulation in the suction pipette recordings (see Fig. 6). The WT OSNs fired action potentials almost exclusively at the first 1 s odour application while the *Tmem16b* KO were firing at each stimulation (Fig. 7A). The number of action potentials and duration of the action potential train was altered in the KO, being, respectively, higher and longer than in the WT (Fig. 7C; number of action potentials WT 3.7 ± 0.8
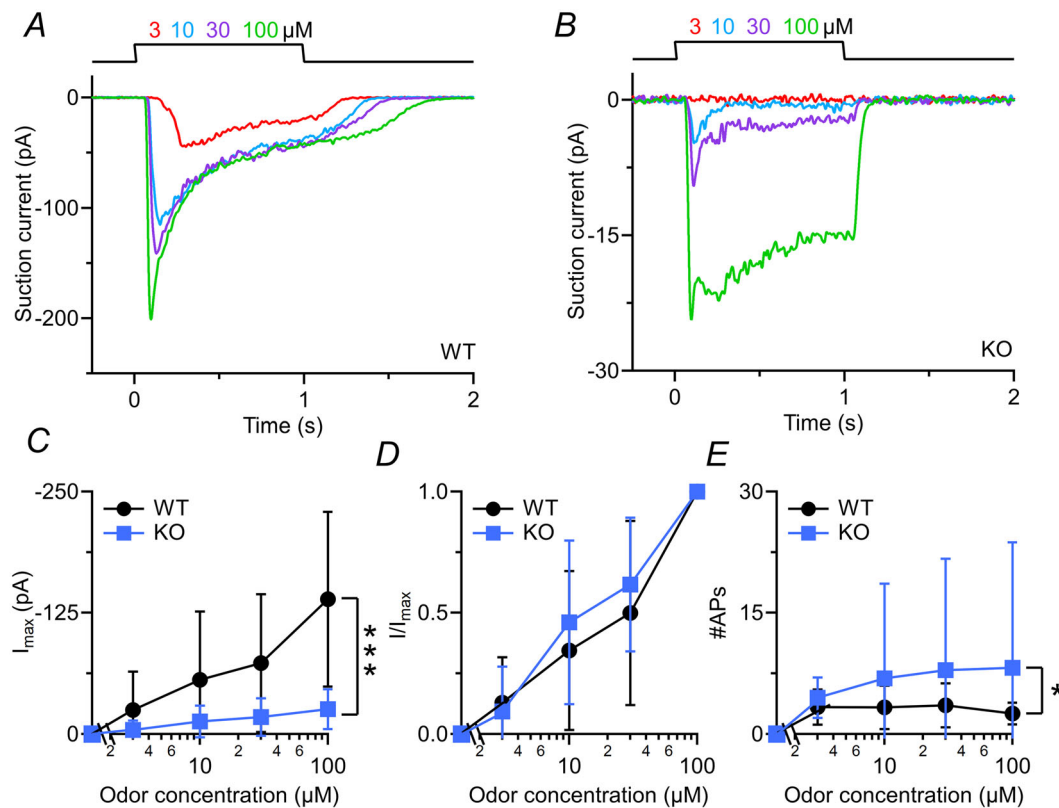

Figure 4. The lack of TMEM16B does not alter the olfactory sensory neuron (OSN) odour sensitivity
A, WT and *B*, *Tmem16b* KO OSNs were stimulated with increasing odorant concentrations at the indicated concentration (mixture of cineole and acetophenone) for 1 s. Responses were recorded from isolated OSNs using the suction pipette technique and filtered 0–50 Hz. *C*, dose–response relationship of the maximal peak current I_{max} with WT being significantly larger (two-way ANOVA, $F_{(1,101)} = 16.63$, $P = 0.0001$). *D*, the dose–response of each OSN was normalized to its response at 100 µM (not different between WT and KO, two-way ANOVA, $F_{(1,101)} = 0.19$, $P = 0.67$). *E*, number of action potentials generated in WT and KO OSNs, which was statistically higher in the KO (two-way ANOVA, $F_{(1,107)} = 23.96$, $P = 0.0106$; $n = 17$–20 for WT and 13–16 for KO). Data points are means ± SD. [Colour figure can be viewed at wileyonlinelibrary.com]

$n = 7$, KO 13 ± 3 $n = 7$, $P = 0.0047$ *U* test; duration WT 144 ± 79 ms $n = 7$, KO 670 ± 176 ms $n = 7$, $P = 0.017$ *U* test). During the first stimulation, the WT decreased its firing frequency and fell silent quickly, while the KO progressively reduced its firing frequency but continued to fire throughout the 1 s stimulation. Interestingly, the lack of silencing did not influence the ability to fire action potentials at each stimulation in the KO. We quantified an adaptation index as a ratio between the number of action potentials in response to the *n*th stimulation and the number of action potentials at the first. The WT OSNs nearly completely stopped firing as the action potentials in the stimulations following the first were very few or even absent (Fig. 7*E*). The KO had a number of action potentials that was about 60% of the first stimulus and it stabilized at around 50% across subsequent stimulations (Fig. 7*E*). In summary, using this stimulation paradigm we conclude that OSNs from *Tmem16b* KO follow the

stimulation with higher fidelity (see also Fig. 6). Because of our perfusion and experimental slice set-up, we could not shorten the inter-pulse interval further. When we increased the interval to 1 s (Fig. 7*B*), we could again observe an increase in the number and action potential train duration in the KO (Fig. 7*D*), but the adaptation index was similar between WT and KO (Fig. 7*F*).

We also performed the same type of stimulation protocol but instead of an odorant mix we used IBMX. The responses in term of number of action potential and action potential train duration were qualitatively similar to those obtained with the odorant mix (Fig. 8*A–F*; number of action potentials WT 6.4 ± 1.6 $n = 12$, KO 14.9 ± 2.6 $n = 12$, $P = 0.0075$ *U* test; duration WT 142 ± 47 ms $n = 12$, KO 819 ± 103 ms $n = 12$, $P = 9 \times 10^{-5}$ *U* test). With an inter-pulse interval of 0.5 s in the WT, few action potentials were reemerging from adaptation in the later pulses, thus increasing the adaptation index compared
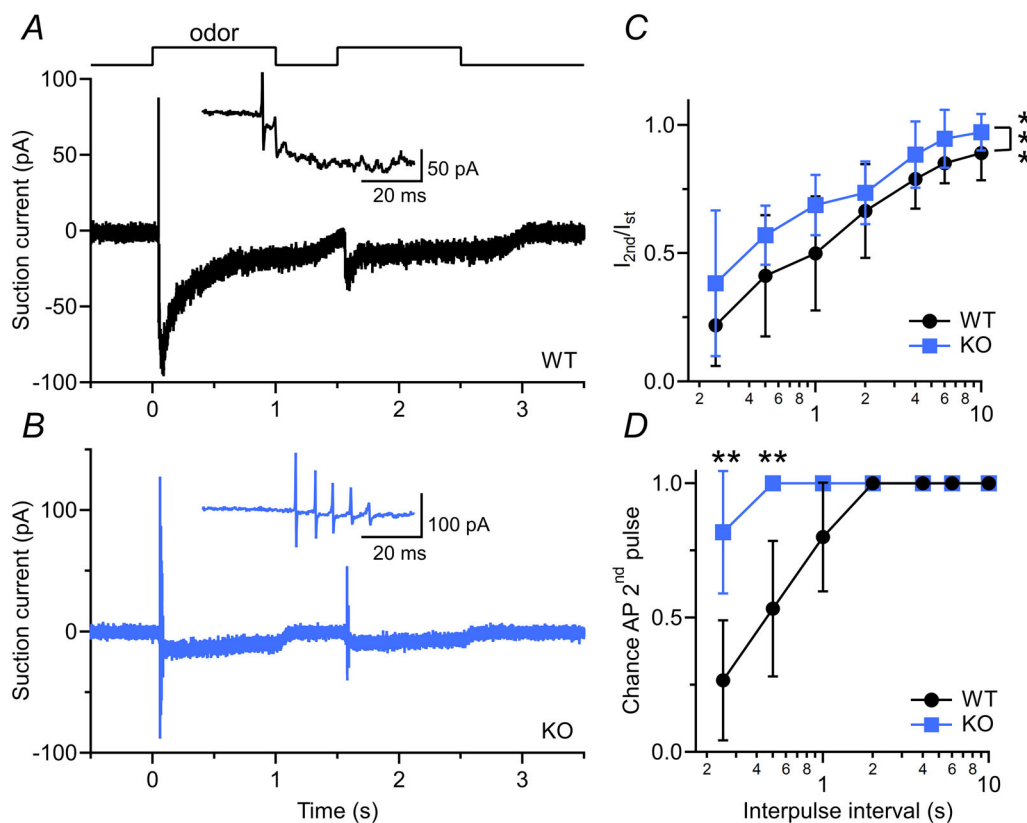

Figure 5. The lack of TMEM16B fastens the recovery from adaptation
Double pulse experiments to determine response recovery following adaptation. *A*, a WT and *B*, *Tmem16b* KO olfactory sensory neuron (OSN) were stimulated twice for 1 s with an inter-pulse time of 0.5 s. Odorants were cineole and acetophenone at 100 μM each, currents were recorded with the suction pipette technique from isolated OSNs and filtered at 0–5 kHz. Note that both WT and KO OSN generated action potentials to the first stimulus, but the WT OSN failed to generate action potentials in response to the second stimulus in contrast to the KO OSN. *C*, for increasing inter-pulse times, the peak current of the second response was normalized to the first response. Data are means ± SD. WT and KO are significantly different, two-way ANOVA, $F_{(1,160)} = 23.96$, $P = 2.3 \times 10^{-6}$. *D*, chance that OSNs fire an action potential in response to the second odorant exposure, data points are means ± 95% confidence interval, ** $P = 0.007$ for 0.25 s and $P = 0.0098$ for 0.5 s, Fisher's exact test. $n = 11$–15 OSNs for WT and KO. [Colour figure can be viewed at wileyonlinelibrary.com]

with that observed with the odorant mix (compare Fig 8*A* with 7*A*). The differences between the adaptation indexes of the WT and the KO were also present, especially at the second and third IBMX applications (Fig. 8*E*). All differences between WT and KO were no longer observed when we increased the stimulus interval to 1 s (Fig. 8*B–F*).

In summary, OSNs from *Tmem16b* KO have altered adaptation properties failing to modulate the number of action potentials and spike train duration according to the stimulation frequency.

Discussion

The events that lead to the generation of the receptor potential in OSN cilia are triggered by the binding of an odorant to the olfactory receptor (OR) and shaped by the currents generated via the cationic CNG channel first and anionic TMEM16B current thereafter. It has long been established that the Cl⁻ current provides high gain, low noise amplification of the receptor current, such that the increase in overall current did not add additional current fluctuations due to the small unitary conductance of the Cl⁻ channel (Kleene, 2008; Li et al., 2018; Lowe & Gold, 1993) The CNG channel's contribution to shaping the time course and overall sensitivity, in particular during repetitive stimulation, has received less attention (Dibattista et al., 2017, 2024; Pifferi et al., 2012).

The Cl⁻ opens following the opening of the CNG channel and Ca^{2+} influx, which is the main source of ciliary Ca^{2+} rises (Boccaccio et al., 2021; Firestein et al., 1991; Kleene, 2008; Lowe & Gold, 1993; Nakamura & Gold, 1987; Schild & Restrepo, 1998). Hence its activation is closely coupled to the activation kinetics of the CNG channel. This is consistent with the here reported similar response delay in both WT and *Tmem16b* KO OSNs and suggests that the response delay is mainly dependent on the speed of generation of the second messenger cAMP and the ensuing activation of the CNG channel. The decline of the odorant response during a 1 s stimulation (Fig. 3*F*) was similar in WT and KO OSNs, suggesting that this form of adaptation is mostly driven by the gating of the CNG channel and thus either via desensitization of the CNG channel or a reduction in available cAMP, either
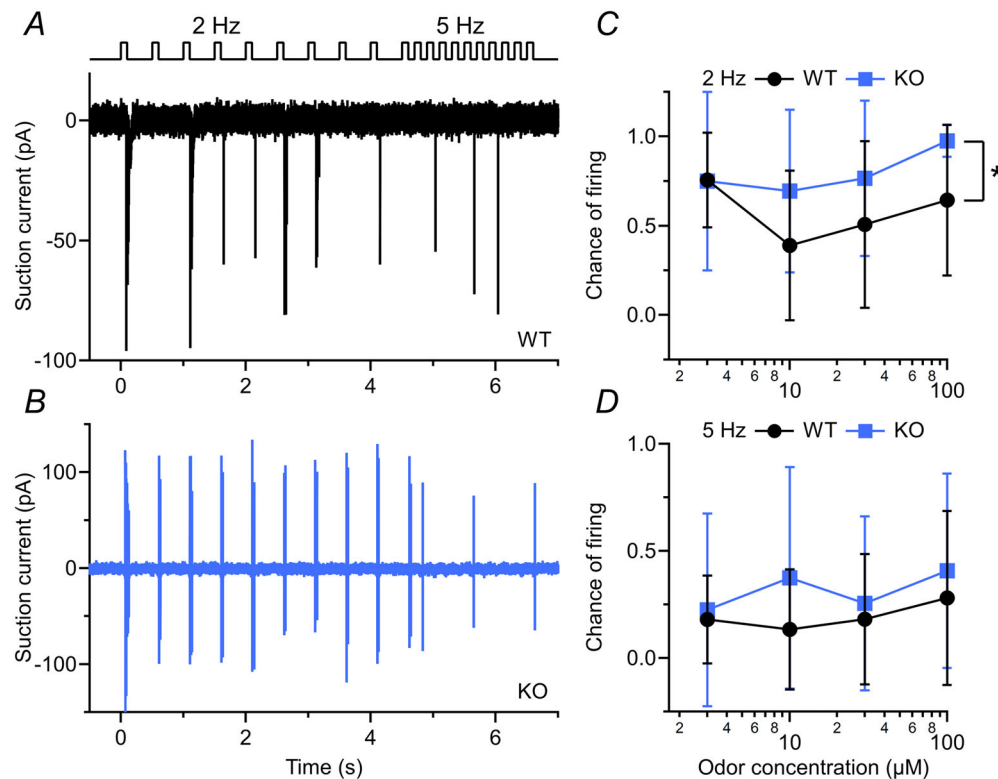

Figure 6. Odorant responses to 2 and 5 Hz stimulations
A, a WT and *B*, *Tmem16b* KO olfactory sensory neuron (OSN) were stimulated at 2 Hz followed by 5 Hz as indicated by the solution monitor at the top (100 ms stimulus duration, 100 μM cineole and acetophenone each). Currents were recorded with the suction pipette technique from isolated OSNs at 0–5 kHz. *C* and *D*, reliability of WT and *Tmem16b* KO OSNs to generate action potentials at each 2 Hz and at 5 Hz stimulation. At 2 Hz, WT and KO are statistically different (two-way ANOVA, $F_{(1,80)} = 67.3$, $P = 0.02$) but not at 5 Hz (two-way ANOVA, $F_{(1,80)} = 1.66$, $P = 0.20$; $n = 5$–20 for WT and 4–14 for KO). Data are means ± SD. [Colour figure can be viewed at wileyonlinelibrary.com]

by reduced cAMP synthesis or increased ciliary cAMP hydrolysis by PDE (Boccaccio et al., 2006, 2021; Cygnar & Zhao, 2009; Dibattista & Reisert, 2016).

Response termination following cessation of odorant stimulation requires the closure of the Cl^- channel. Which itself depends on the closure of the CNG channel and cessation of Ca^{2+} influx and additionally on the removal of ciliary Ca^{2+}, the latter uncoupling the Cl^- channel from CNG channel kinetics. It has long been known that when inhibiting Ca^{2+} extrusion by removing extracellular Na^+, thus abolishing the driving force of Na^+-dependent Ca^{2+} extrusion, the response is greatly prolonged and carried by a sustained Ca^{2+}-activated Cl^- current (Antolin & Matthews, 2007; Jung et al., 1994;

Reisert & Matthews, 1998, 2001). The main molecular determinant of Ca^{2+} extrusion is the K^+-dependent Na^+/Ca^{2+} exchanger 4 (NCKX4) and *Nckx4* knockout OSNs display prolonged response termination by up to several seconds (Stephan et al., 2011). Here, in the *Tmem16b* KO, we observed a faster response termination than in the WT, consistent with the view that it is the Cl^- current that determines the duration of the response. Interestingly and importantly, the rate of termination also determines recovery from adaptation during repetitive odorant stimulation (Dibattista & Reisert, 2016; Stephan et al., 2011). It is a key cellular behaviour for OSNs to fine-tune their dynamic response across various input levels, both in stimulation magnitude as well as
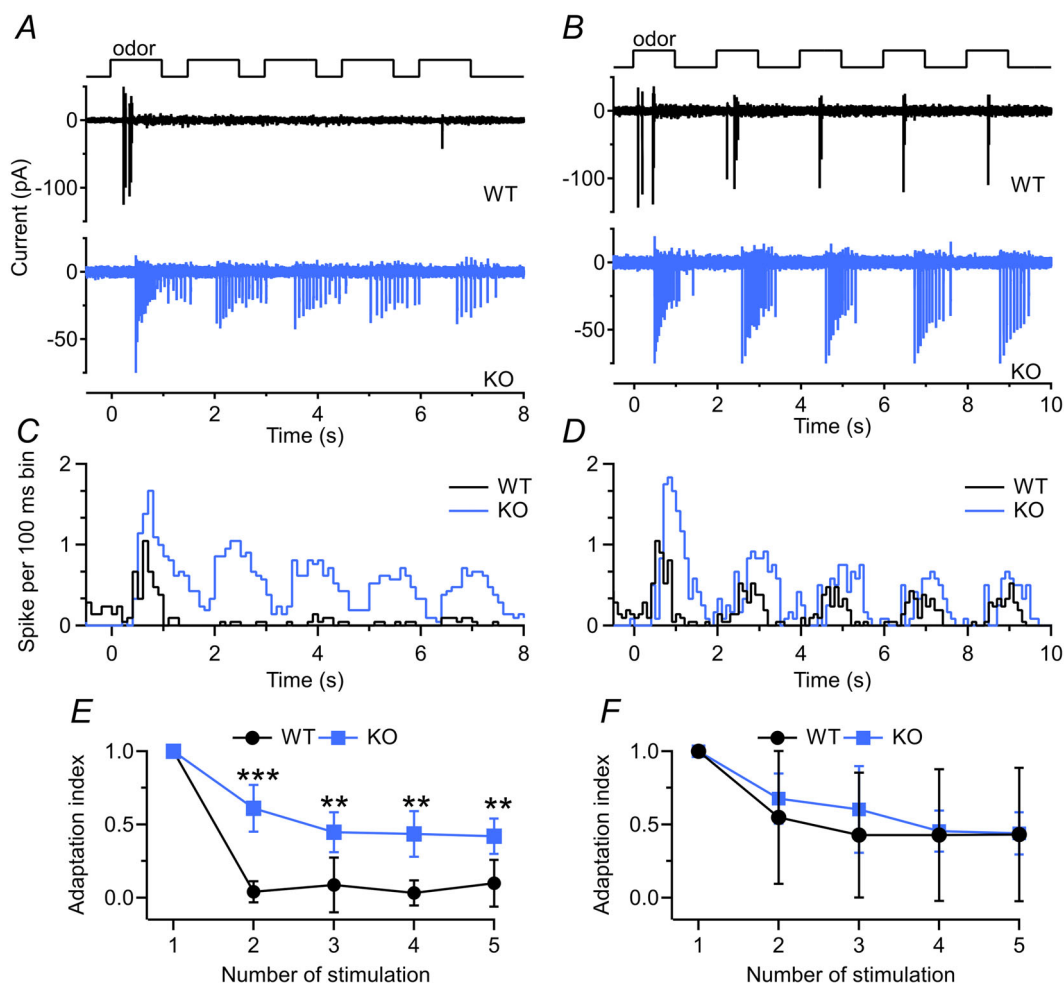

Figure 7. The lack of TMEM16B fastens the recovery from adaptation after odour stimulation in loose-patch recording
Representative loose-patch recordings from olfactory sensory neurons (OSNs) in olfactory epithelia (OE) slices from WT and *Tmem16b* KO mice stimulated with an odour mix five times with an inter-pulse interval of 0.5 s (*A*) or 1 s (*B*). *C* and *D*, peristimulus histograms showing the sum of number of spikes for all the cells normalized by the number of cells (bin = 100 ms) for experiments in *A* and *B* (*n* = 7 for WT and KO). *E* and *F*, adaptation index (ratio of action potentials evoked by the *n*th stimulation and the number of action potentials evoked by first stimulation) from experiments in *A* and *B* (*n* = 7 for WT and *n* = 4 KO; *E*: 2nd: *P* = 0.00058; 3rd: 0.0099; 4th: 0.001; 5th: 0.004; *F*: 2nd: *P* = 0.38; 3rd: *P* = 0.24; 4th: *P* = 0.5; 5th: *P* = 0.6; *** *P* < 0.001 ** *P* < 0.01 *U* test). [Colour figure can be viewed at wileyonlinelibrary.com]

stimulation frequency, the latter varying with the sniffing frequency of the mouse (Firestein et al., 1990; Ghatpande & Reisert, 2011). In particular, adaptation to repeated stimuli manifests as a reduction in the current amplitude of the response to the second odorant stimulus with respect to the first (Boccaccio et al., 2006; Song et al., 2008; Stephan et al., 2011). This difference in amplitude of the responses is reduced when the time interval between stimuli is increased; complete recovery of the response is seen for a sufficiently long interval. We show here that the *Tmem16b* KO response recovery is faster than in the WT, meaning that for a given inter-pulse interval, the response to the second stimulation in a *Tmem16b* KO regains a larger amplitude normalized to the first when compared with the WT. This could be explained in at least

two not-mutually exclusive ways. The Cl^- channel itself might undergo inactivation during prolonged increased Ca^{2+} levels, for which there is evidence that this is the case (Ponissery Saidu et al., 2013; Reisert et al., 2003). Alternatively, as overall current levels, and therefore cellular depolarization, are changed in the *Tmem16b* KO, this will also alter Ca^{2+} influx and ciliary Ca^{2+} levels that could lead to altered adaptation of the transduction cascade by, for example, altering the CNG channel's sensitivity to cAMP (Bradley et al., 2004; Song et al., 2008). As stated above, response termination is important to determine adaptation, and *Nckx4* KO OSNs showed that NCKX4 is required to lower intraciliary Ca^{2+} during and after odorant stimulation, allowing the transduction cascade to recover from adaptation (Stephan et al., 2011).
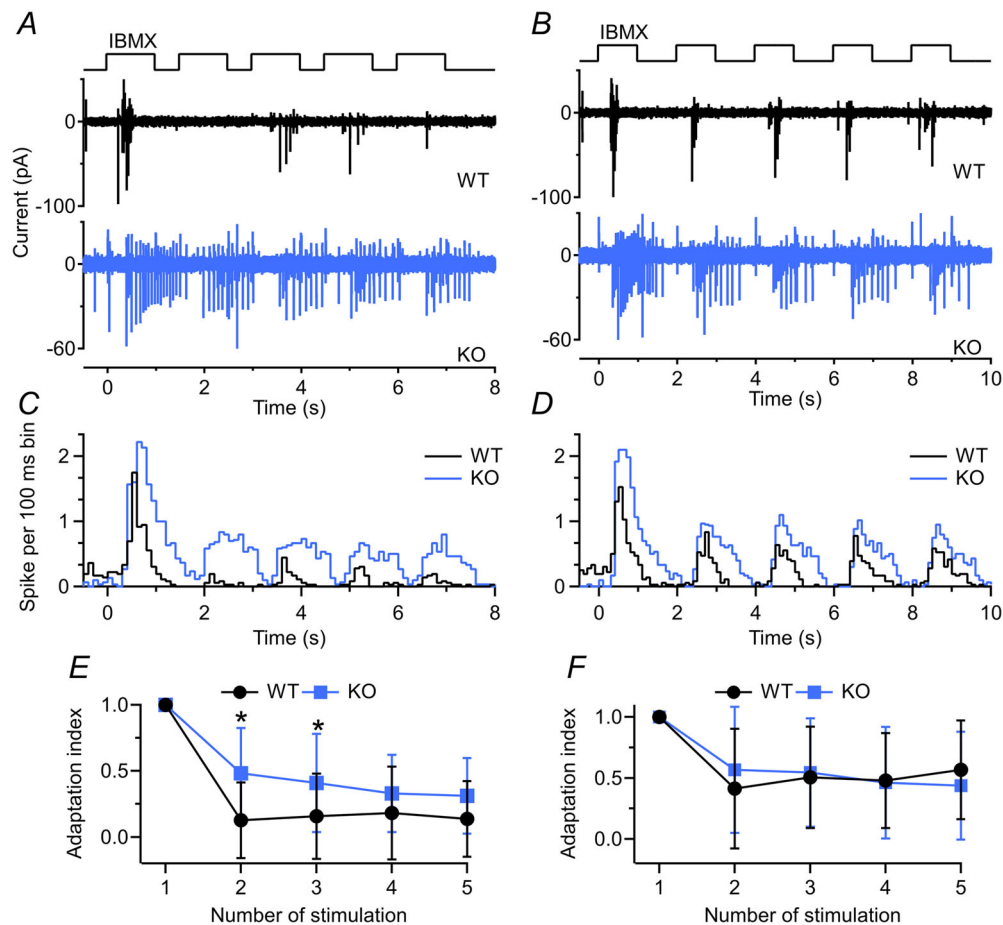

Figure 8. The lack of TMEM16B fastens the recovery from adaptation after IBMX stimulation in loose-patch recording
Representative loose-patch recordings of olfactory sensory neurons (OSNs) in olfactory epithelia (OE) slices from WT and *Tmem16b* KO mice stimulated with 1 mM IBMX five times with an inter-pulse interval of 0.5 s (*A*) or 1 s (*B*). *C* and *D*, peristimulus histograms showing the sum of number of spikes for all the cells normalized by the number of cells (bin = 100 ms) for experiments in *A* and *B* (*n* = 12 for WT and *n* = 10 for KO). *E* and *F*, adaptation index (ratio of action potentials evoked by the *n*th stimulation and the number of action potentials evoked by first stimulation) from experiments in *A* and *B* (*n* = 12 for WT and *n* = 10 for KO; *E*: 2nd: *P* = 0.01; 3rd: 0.02; 4th: 0.06; 5th: 0.07; *F*: 2nd: *P* = 0.42; 3rd: *P* = 0.96; 4th: *P* = 0.83; 5th: *P* = 0.53; **P* < 0.05 *U* test). [Colour figure can be viewed at wileyonlinelibrary.com]

While it has long been established that the Cl^- current amplifies the odorant response (Boccaccio & Menini, 2007; Kleene, 1993; Reisert et al., 2005), it remains unclear whether OSNs alter their odorant sensitivity in the absence of the Cl^- channel. We performed odorant dose–response experiments and, as expected, WT odorant responses were larger than the KO's. But normalization of the responses to their maximal current revealed that WT and KO dose–response relationships overlap and are not shifted relative to each other. This suggests that the sensitivity of OSNs is mostly determined by events upstream of the Cl^- channel and that odorant sensitivity does not seem to be affected by the lack of the Cl^- current. These results seem to disagree with the idea that the Cl^- current may non-linearly amplify small OSN responses as the Ca^{2+}-activated Cl^- current is highly cooperative (Li et al., 2016, 2018; Lowe & Gold, 1993). A potential explanation of the observed differences is that previous work was performed in voltage-clamped OSNs, while in our experiments, the voltage was free to vary, which might limit the amount of current an OSN can generate (Lowe & Gold, 1993). Experiments using suction pipette recordings were performed at room temperature which makes them difficult to compare with ours (Li et al., 2018). A potential caveat here is that the OSNs we recorded from were randomly selected and we used a mix of cineole and acetophenone as the stimulating odorants. Thus, we have taken an 'odour-centric' approach to the question but have not addressed this question in an 'OR-centric' perspective, where one would record from OSNs expressing known ORs.

The action potentials constitute the output of OSNs that are being sent to the olfactory bulb. OSNs increase their firing rate upon increasing odorant concentration. The number of action potentials, though, first increases monotonically with increasing concentration, but reaches a plateau or even decreases at higher odorant concentrations (Reisert & Matthews, 2001; Rospars et al., 2008). Interestingly, OSNs fire action potentials only in the very early phase of the odorant response in isolated OSNs, usually generating two or three action potentials; rarely five or more due to a rapidly declining action potential amplitude brought on by inactivation of voltage-gated Na^+ and Ca^{2+} channels (Pietra et al., 2016; Trotier, 1994). Only when recording from OSNs of *Tmem16B* KO does this number increase to eight (or more) during dose–response experiments. It should be mentioned again that we recorded from OSNs which expressed an unknown OR with unknown sensitivity to the applied odorants. Nevertheless, WT OSNs showed a narrow range of fired action potentials, indicating the robustness of this mechanism over the sensitivity range of an OSN. This range of fired action potentials widened in the KO, with some OSNs showing a very high number of fired action potentials. Which might explain

our observation that at a single odorant concentration in Fig. 3*L* (unlike across a range of applied concentrations, Fig. 4*E*), the difference between WT and KO has not reached statistical significance.

Triggering action potentials also depends on the input resistance of the OSNs, which is high overall and small currents are sufficient to elicit action potential firing (Kleene, 2008; Lynch & Barry, 1989). We did not detect any substantial changes either in voltage-gated currents or in input resistance between WT and KO. Therefore, similar input resistance of OSNs from WT and KO guarantee that the current needed to trigger action potentials would be substantially the same. The increase in the number of action potentials that we observed in the *Tmem16b* KO may be due to the slower rise rate (slope) of the receptor current in the KO rather than its overall time course.

The termination of the receptor current is important for odorant perception during repeated stimulation. In our double-pulse paradigm, for short inter-pulse intervals of 0.5 s, around 50% of WT OSNs failed to generate action potentials in response to the second stimulation but reliably improve when the inter-pulse interval is lengthened. An increase in stimulation frequency (shorter inter-pulse interval) progressively abolished action potential generation. *Tmem16b* KO OSNs were able to fire action potentials reliably (close to 100%) even at the shortest (0.25 s) inter-pulse interval. We investigated OSN firing behaviour in more detail by shortening both stimulus duration and the inter-pulse interval so that our protocol mimicked normal breathing (2 Hz) and higher-frequency sniffing (5 Hz) and recording with the suction pipette technique. We observed that *Tmem16b* KO OSNs generated action potentials more faithfully than WT in response to 2 Hz stimuli. Thus, similar to the results in the double-pulse experiments, lack of Cl^- current apparently allows OSNs to track stimulations more reliably. At 5 Hz, both WT and KO OSNs tracked stimulations only poorly, suggesting that the faster response termination seen in the KO can no longer compensate for the higher stimulation frequency. Nevertheless, it might seem counterintuitive that the lack of the Cl^- channel, and a great reduction in depolarizing current, yields an OSN that generates more action potentials more reliable during repeated stimulation, an observation consistent with the observed larger responses when imaging from OSN axon terminals in the OB of *Tmen16b* KO mice (Zak et al., 2018). Or in other words, why does the addition of a Cl^- current in OSNs seem to abolish encoding of odour stimuli during repeated stimulation? An interesting notion here is the concept of adaptive filtering (Ghatpande & Reisert, 2011). As mice are able to modulate their breathing frequency and hence the stimulation frequency of their own OSNs, they can also alter the olfactory information they receive with an

increase in breathing frequency suppressing the sensation of present odorants, but still enable the perception of new odorants. Our data suggest that the Cl$^-$ could be an important, if not the determining, component in such a mechanism. They might also explain an apparent discrepancy between behavioural deficits reported for *Tmem16b* KO mice. In Go/Nogo experiments, mice show no behavioural deficits in odour discrimination and sensitivity (Billig et al., 2011), while in food search tasks, where mice had to locate a scented food item buried under the bedding in their cage, KO mice performed worse than WT (Neureither et al., 2017; Pietra et al., 2016). A potential explanation is that in the Go/Nogo task only the first inhalation and therefore first odour stimulation, which will generate action potentials reliably both in WT and KO OSNs, might suffice to perform the odour identification task, which can be conducted in as short as 200 ms (Abraham et al., 2004; Rinberg et al., 2006; Uchida & Mainen, 2003). In the search task, repeated odour sampling over time is required, which is heavily altered in the *Tmem16b* KO OSNs as we show here.

In summary, most of the response characteristics of the odorant response in OSNs depend on the Cl$^-$ current. Therefore, it not only amplifies the odorant response, but also shapes response kinetics acting synergistically with NCKX4 in determining the optimal rate of termination. By doing so, they control cellular properties that are directly linked to response termination such as adaptation to repeated stimulation.

References

Abraham, N. M., Spors, H., Carleton, A., Margrie, T. W., Kuner, T., & Schaefer, A. T. (2004). Maintaining accuracy at the expense of speed. *Neuron*, **44**, 865–876.

Agostinelli, E., Gonzalez-Velandia, K. Y., Hernandez-Clavijo, A., Kumar Maurya, D., Xerxa, E., Lewin, G. R., Michele, D., Menini, A., & Pifferi, S. (2021). A role for STOML3 in olfactory sensory transduction. *eNeuro*, **8**(2). https://doi.org/10.1523/ENEURO.0565-20.2021

Antolin, S., & Matthews, H. R. (2007). The effect of external sodium concentration on sodium–calcium exchange in frog olfactory receptor cells. *The Journal of Physiology*, **581**(2), 495–503.

Bakalyar, H. A., & Reed, R. R. (1990). Identification of a specialized adenylyl cyclase that may mediate odorant detection. *Science*, **250**(4986), 1403–1406.

Belluscio, L., Gold, G. H., Nemes, A., & Axel, R. (1998). Mice Deficient in Golf Are Anosmic. *Neuron*, **20**(1), 69–81.

Billig, G. M., Pál, B., Fidzinski, P., & Jentsch, T. J. (2011). Ca^{2+}-activated Cl$^-$ currents are dispensable for olfaction. *Nature Neuroscience*, **14**(6), 763–769.

Boccaccio, A., Lagostena, L., Hagen, V., & Menini, A. (2006). Fast adaptation in mouse olfactory sensory neurons does not require the activity of phosphodiesterase. *Journal of General Physiology*, **128**(2), 171–184.

Boccaccio, A., & Menini, A. (2007). Temporal development of cyclic nucleotide-gated and Ca^{2+}-activated Cl$^-$ currents in isolated mouse olfactory sensory neurons. *Journal of Neurophysiology*, **98**(1), 153–160.

Boccaccio, A., Menini, A., & Pifferi, S. (2021). The cyclic AMP signaling pathway in the rodent main olfactory system. *Cell and Tissue Research*, **383**(1), 429–443.

Bradley, J., Bönigk, W., Yau, K.-W., & Frings, S. (2004). Calmodulin permanently associates with rat olfactory CNG channels under native conditions. *Nature Neuroscience*, **7**(7), 705–710.

Brunet, L. J., Gold, G. H., & Ngai, J. (1996). General anosmia caused by a targeted disruption of the mouse olfactory cyclic nucleotide–gated cation channel. *Neuron*, **17**(4), 681–693.

Buck, L., & Axel, R. (1991). A novel multigene family may encode odorant receptors: A molecular basis for odor recognition. *Cell*, **65**(1), 175–187,

Cang, J., & Isaacson, J. S. (2003). In vivo whole-cell recording of odor-evoked synaptic transmission in the rat olfactory bulb. *Journal of Neuroscience*, **23**(10), 4108–4116.

Cygnar, K. D., & Zhao, H. (2009). Phosphodiesterase 1C is dispensable for rapid response termination of olfactory sensory neurons. *Nature Neuroscience*, **12**(4), 454–462.

Dibattista, M., Mazzatenta, A., Grassi, F., Tirindelli, R., & Menini, A. (2008). Hyperpolarization-activated cyclic nucleotide-gated channels in mouse vomeronasal sensory neurons. *Journal of Neurophysiology*, **100**(2), 576–586.

Dibattista, M., Pifferi, S., Boccaccio, A., Menini, A., & Reisert, J. (2017). The long tale of the calcium activated Cl(−) channels in olfactory transduction. *Channels (Austin)*, 1–16.

Dibattista, M., Pifferi, S., Hernandez-Clavijo, A., & Menini, A. (2024). The physiological roles of anoctamin2/TMEM16B and anoctamin1/TMEM16A in chemical senses. *Cell Calcium*, **120**, 102889.

Dibattista, M., & Reisert, J. (2016). The odorant receptor-dependent role of olfactory marker protein in olfactory receptor neurons. *Journal of Neuroscience*, **36**(10), 2995–3006.

Dibattista, M., & Reisert, J. (2018). Suction Pipette technique: An electrophysiological tool to study olfactory receptor-dependent signal transduction. *Methods in Molecular Biology*, **1820**, 137–145.

Firestein, S., Shepherd, G. M., & Werblin, F. S. (1990). Time course of the membrane current underlying sensory transduction in salamander olfactory receptor neurones. *The Journal of Physiology*, **430**(1), 135–158.

Firestein, S., Zufall, F., & Shepherd, G. M. (1991). Single odor-sensitive channels in olfactory receptor neurons are also gated by cyclic nucleotides. *Journal of Neuroscience*, **11**(11), 3565–3572.

Genovese, F., Reisert, J., & Kefalov, V. J. (2021). Sensory transduction in photoreceptors and olfactory sensory neurons: Common features and distinct characteristics. *Frontiers in Cellular Neuroscience*, **15**, 761416.

Ghatpande, A. S., & Reisert, J. (2011). Olfactory receptor neuron responses coding for rapid odour sampling. *The Journal of Physiology*, **589**(9), 2261–2273.

Gire, D. H., Franks, K. M., Zak, J. D., Tanaka, K. F., Whitesell, J. D., Mulligan, A. A., Hen, R., & Schoppa, N. E. (2012). Mitral cells in the olfactory bulb are mainly excited through a multistep signaling path. *Journal of Neuroscience*, **32**(9), 2964–2975.

Guarneri, G., Pifferi, S., Dibattista, M., Reisert, J., & Menini, A. (2023). Paradoxical electro-olfactogram responses in TMEM16B knock-out mice. *Chemical Senses*, **48**, bjad003.

Hengl, T., Kaneko, H., Dauner, K., Vocke, K., Frings, S., & Möhrlen, F. (2010). Molecular components of signal amplification in olfactory sensory cilia. *Proceedings of the National Academy of Sciences of the United States of America*, **107**(13), 6052–6057.

Henriques, T., Agostinelli, E., Hernandez-Clavijo, A., Maurya, D. K., Rock, J. R., Harfe, B. D., Menini, A., & Pifferi, S. (2019). TMEM16A calcium-activated chloride currents in supporting cells of the mouse olfactory epithelium. *Journal of General Physiology*, **151**(7), 954–966.

Jones, D. T., & Reed, R. R. (1989). Golf: An olfactory neuron specific-G protein involved in odorant signal transduction. *Science*, **244**(4906), 790–795.

Jung, A., Lischka, F. W., Engel, J., & Schild, D. (1994). Sodium/calcium exchanger in olfactory receptor neurones of *Xenopus laevis*. *Neuroreport*, **5**(14), 1741–1744.

Kaneko, H., Putzier, I., Frings, S., Kaupp, U. B., & Gensch, T. (2004). Chloride accumulation in mammalian olfactory sensory neurons. *Journal of Neuroscience*, **24**(36), 7931–7938.

Kawai, F., Kurahashi, T., & Kaneko, A. (1997). Quantitative analysis of Na^+ and Ca^{2+} current contributions on spike initiation in the newt olfactory receptor cell. *The Japanese Journal of Physiology*, **47**(4), 367–376.

Kleene, S. J. (1993). Origin of the chloride current in olfactory transduction. *Neuron*, **11**(1), 123–132.

Kleene, S. J. (2008). The electrochemical basis of odor transduction in vertebrate olfactory cilia. *Chemical Senses*, **33**(9), 839–859.

Kleene, S., & Gesteland, R. (1991). Calcium-activated chloride conductance in frog olfactory cilia. *Journal of Neuroscience*, **11**(11), 3624–3629.

Kurahashi, T., & Yau, K.-W. (1993). Co-existence of cationic and chloride components in odorant-induced current of vertebrate olfactory receptor cells. *Nature*, **363**(6424), 71–74.

Li, R.-C., Ben-Chaim, Y., Yau, K.-W., & Lin, C.-C. (2016). Cyclic-nucleotide–gated cation current and Ca^{2+}-activated Cl current elicited by odorant in vertebrate olfactory receptor neurons. *Proceedings of the National Academy of Sciences of the United States of America*, **113**(40), 11078–11087.

Li, R.-C., Lin, C.-C., Ren, X., Wu, J. S., Molday, L. L., Molday, R. S., & Yau, K.-W. (2018). Ca^{2+}-activated Cl current predominates in threshold response of mouse olfactory receptor neurons. *Proceedings of the National Academy of Sciences*, **115**(21), 5570–5575.

Lowe, G., & Gold, G. H. (1991). The spatial distributions of odorant sensitivity and odorant-induced currents in salamander olfactory receptor cells. *The Journal of Physiology*, **442**(1), 147–168.

Lowe, G., & Gold, G. H. (1993). Nonlinear amplification by calcium-dependent chloride channels in olfactory receptor cells. *Nature*, **366**(6452), 283–286.

Lynch, J. W., & Barry, P. H. (1989). Action potentials initiated by single channels opening in a small neuron (rat olfactory receptor). *Biophysical Journal*, **55**(4), 755–768.

Malnic, B., Hirono, J., Sato, T., & Buck, L. B. (1999). Combinatorial receptor codes for odors. *Cell*, **96**(5), 713–723.

Matthews, H. (1999). A compact modular flow heater for the superfusion of mammalian cells. *The Journal of Physiology*, **518**, 13P.

Maurya, D. K., Henriques, T., Marini, M., Pedemonte, N., Galietta, L. J. V., Rock, J. R., Harfe, B. D., & Menini, A. (2015). Development of the olfactory epithelium and nasal glands in TMEM16A$^{-/-}$ and TMEM16A$^{+/+}$ Mice. *PLoS One*, **10**(6), e0129171.

Maurya, D. K., & Menini, A. (2014). Developmental expression of the calcium-activated chloride channels TMEM16A and TMEM16B in the mouse olfactory epithelium. *Developmental Neurobiology*, **74**(7), 657–675.

Nakamura, T., & Gold, G. H. (1987). A cyclic nucleotide-gated conductance in olfactory receptor cilia. *Nature*, **325**(6103), 442–444.

Neureither, F., Stowasser, N., Frings, S., & Möhrlen, F. (2017). Tracking of unfamiliar odors is facilitated by signal amplification through anoctamin 2 chloride channels in mouse olfactory receptor neurons. *Physiological Reports*, **5**(15), e13373.

Pietra, G., Dibattista, M., Menini, A., Reisert, J., & Boccaccio, A. (2016). The Ca^{2+}-activated Cl^- channel TMEM16B regulates action potential firing and axonal targeting in olfactory sensory neurons. *The Journal of General Physiology*, **148**(4), 293–311.

Pifferi, S., Cenedese, V., & Menini, A. (2012). Anoctamin 2/TMEM16B: A calcium-activated chloride channel in olfactory transduction. *Experimental Physiology*, **97**(2), 193–199.

Ponissery Saidu, S., Dibattista, M., Matthews, H. R., & Reisert, J. (2012). Odorant-induced responses recorded from olfactory receptor neurons using the suction pipette technique. *Journal of Visualized Experiments: JoVE*, e3862.

Ponissery Saidu, S., Stephan, A. B., Talaga, A. K., Zhao, H., & Reisert, J. (2013). Channel properties of the splicing isoforms of the olfactory calcium-activated chloride channel Anoctamin 2. *Journal of General Physiology*, **141**(6), 691–703.

Rasche, S., Toetter, B., Adler, J., Tschapek, A., Doerner, J. F., Kurtenbach, S., Hatt, H., Meyer, H., Warscheid, B., & Neuhaus, E. M. (2010). Tmem16b is specifically expressed in the cilia of olfactory sensory neurons. *Chemical Senses*, **35**(3), 239–245.

Reisert, J., Bauer, P. J., Yau, K.-W., & Frings, S. (2003). The Ca-activated Cl channel and its control in rat olfactory receptor neurons. *Journal of General Physiology*, **122**(3), 349–364.

Reisert, J., Lai, J., Yau, K.-W., & Bradley, J. (2005). Mechanism of the excitatory Cl^- response in mouse olfactory receptor neurons. *Neuron*, **45**(4), 553–561.

Reisert, J., & Matthews, H. R. (1998). Na$^+$-dependent Ca^{2+} extrusion governs response recovery in frog olfactory receptor cells. *Journal of General Physiology*, **112**(5), 529–535.

Reisert, J., & Matthews, H. R. (2001). Response properties of isolated mouse olfactory receptor cells. *The Journal of Physiology*, **530**(1), 113–122.

Reisert, J., Yau, K.-W., & Margolis, F. L. (2007). Olfactory marker protein modulates the cAMP kinetics of the odour-induced response in cilia of mouse olfactory receptor neurons. *The Journal of Physiology*, **585**(3), 731–740.

Rinberg, D., Koulakov, A., & Gelperin, A. (2006). Speed-accuracy tradeoff in olfaction. *Neuron*, **51**(3), 351–358.

Rospars, J.-P., Lansky, P., Chaput, M., & Duchamp-Viret, P. (2008). Competitive and noncompetitive odorant interactions in the early neural coding of odorant mixtures. *Journal of Neuroscience*, **28**(10), 2659–2666.

Sagheddu, C., Boccaccio, A., Dibattista, M., Montani, G., Tirindelli, R., & Menini, A. (2010). Calcium concentration jumps reveal dynamic ion selectivity of calcium-activated chloride currents in mouse olfactory sensory neurons and TMEM16b-transfected HEK 293T cells. *The Journal of Physiology*, **588**(21), 4189–4204.

Schild, D., & Restrepo, D. (1998). Transduction mechanisms in vertebrate olfactory receptor cells. *Physiological Reviews*, **78**(2), 429–466.

Song, Y., Cygnar, K. D., Sagdullaev, B., Valley, M., Hirsh, S., Stephan, A., Reisert, J., & Zhao, H. (2008). Olfactory CNG channel desensitization by Ca^{2+}/CaM via the B1b subunit affects response termination but not sensitivity to recurring stimulation. *Neuron*, **58**(3), 374–386.

Spors, H., Wachowiak, M., Cohen, L. B., & Friedrich, R. W. (2006). Temporal dynamics and latency patterns of receptor neuron input to the olfactory bulb. *Journal of Neuroscience*, **26**(4), 1247–1259.

Stephan, A. B., Shum, E. Y., Hirsh, S., Cygnar, K. D., Reisert, J., & Zhao, H. (2009). ANO2 is the cilial calcium-activated chloride channel that may mediate olfactory amplification. *Proceedings of the National Academy of Sciences of the United States of America*, **106**(28), 11776–11781.

Stephan, A. B., Tobochnik, S., Dibattista, M., Wall, C. M., Reisert, J., & Zhao, H. (2011). The Na(+)/Ca(2+) exchanger NCKX4 governs termination and adaptation of the mammalian olfactory response. *Nature Neuroscience*, **15**(1), 131–137.

Tan, L., Li, Q., & Xie, X. S. (2015). Olfactory sensory neurons transiently express multiple olfactory receptors during development. *Molecular Systems Biology*, **11**(12), 844.

Tirindelli, R., Dibattista, M., Pifferi, S., & Menini, A. (2009). From pheromones to behavior. *Physiological Reviews*, **89**(3), 921–956.

Trotier, D. (1994). Intensity coding in olfactory receptor cells. *Seminars in Cell Biology*, **5**(1), 47–54.

Uchida, N., & Mainen, Z. F. (2003). Speed and accuracy of olfactory discrimination in the rat. *Nature Neuroscience*, **6**(11), 1224–1229.

Wong, S. T., Trinh, K., Hacker, B., Chan, G. C. K., Lowe, G., Gaggar, A., Xia, Z., Gold, G. H., & Storm, D. R. (2000). Disruption of the type III adenylyl cyclase gene leads to peripheral and behavioral anosmia in transgenic mice. *Neuron*, **27**(3), 487–497.

Zak, J. D., Grimaud, J., Li, R.-C., Lin, C.-C., & Murthy, V. N. (2018). Calcium-activated chloride channels clamp odor-evoked spike activity in olfactory receptor neurons. *Scientific Reports*, **8**(1), 10600.

Zhang, Y., Zhang, Z., Xiao, S., Tien, J., Le, S., Le, T., Jan, L. Y., & Yang, H. (2017). Inferior olivary TMEM16B mediates cerebellar motor learning. *Neuron*, **95**(5), 1103.

Additional information

Data availability statement

The data that support the findings of this study are available from the first and corresponding authors upon reasonable request.

Competing interests

None declared.

Author contributions

J.R. performed the suction pipette electrophysiological experiments. G.G. and C.R. performed the whole-epithelium and whole-cell electrophysiological experiments. J.R., S.P., A.M. and M.D. conceptualized and analysed the experiments and wrote the manuscript. All the authors approved the final version of the manuscript.

Funding

Acknowledgements

Keywords

calcium-activated chloride current, olfaction, sensory transduction

Supporting information

Additional supporting information can be found online in the Supporting Information section at the end of the HTML view of the article. Supporting information files available:

Peer Review History